## ▌Catalysis

# A State-of-the-Art Heterogeneous Catalyst for Efficient and General Nitrile Hydrogenation

Dario Formenti,[a] Rita Mocci,[a, c] Hanan Atia,[a] Sarim Dastgir,[b] Muhammad Anwar,[b] Stephan Bachmann,[d] Michelangelo Scalone,[d] Kathrin Junge,[a] and Matthias Beller*[a]

**Abstract:** Cobalt-doped hybrid materials consisting of metal oxides and carbon derived from chitin were prepared, characterized and tested for industrially relevant nitrile hydrogenations. The optimal catalyst supported onto MgO showed, after pyrolysis at 700 °C, magnesium oxide nanocubes decorated with carbon-enveloped Co nanoparticles. This special structure allows for the selective hydrogenation of diverse and demanding nitriles to the corresponding primary amines under mild conditions (e.g. 70 °C, 20 bar $H_2$). The advantage of this novel catalytic material is showcased for industrially important substrates, including adipodinitrile, picolinonitrile, and fatty acid nitriles. Notably, the developed system outperformed all other tested commercial catalysts, for example, Raney Nickel and even noble-metal-based systems in these transformations.

## Introduction

Catalysis in all its aspects plays a fundamental role in the development of green chemical transformations. So far, most of the efforts focused on the design of sustainable processes using renewable chemical platforms, benign solvents, and/or earth-abundant catalysts under mild and safe conditions with the aim of minimizing wastes and energy consumption. Nevertheless, less attention has been paid to the catalyst development using earth-abundant and renewable starting materials. In the last decade, transition-metals nanoparticles or single metal atoms (mainly based on Fe, Co, Ni) supported onto nitrogen-doped modified carbon materials have been disclosed as very successful catalytic materials for various selective organic transformations.[1] They are typically prepared by the pyrolysis of well-defined metal complexes or chelates employing nitro-

gen donor ligands, metal-organic frameworks or coordination polymers as precursors. A drawback of this approach lays in the relatively high cost of this nitrogen-containing molecules that could limit the applicability on a large scale. Thus, the synthesis of (doped)-carbonaceous materials starting from sustainable resources is of increasing interest.[2] In this respect, abundantly available cellulose, chitin, and lignin constitute "ideal" candidates for new catalyst developments. Specifically, chitin is the second most abundant biopolymer on Earth and represents a biocompatible nitrogen-containing precursor directly available from crustacean shells. It shows an irrelevant toxicity and hazardousness making its environmental impact negligible.[3]

Recently, our group prepared new materials by pyrolysis of Co salts and chitosan, which is obtained by deacetylation of chitin using large amount of aqueous sodium hydroxide. Interesting activities have been observed in the selective hydrogenation of nitroarenes[4] and olefins,[5] and hydrodehalogenation of aryl and alkyl halides.[6] In continuation with this topic, herein we report unique nanostructured catalysts, whereby cobalt is supported on metal oxide-carbon composites derived from chitin. The optimal material outperforms representative catalysts for industrially relevant hydrogenation of nitriles under the investigated conditions.

## Results and Discussion

In recent years, nanostructured carbon–metal oxide composite materials have gained attention mainly for energy-related applications.[7] Notably, such materials have been scarcely explored in chemical catalysis.[8] In this respect, we envisioned the exploitation of new biomass-derived carbon-metal/metal oxide composites for sustainable redox transformations. Inspired by the preparation of chitosan-derived metal nanoparti-

[a] Dr. D. Formenti, Dr. R. Mocci, Dr. H. Atia, Dr. K. Junge, Prof. Dr. M. Beller
Leibniz-Institut für Katalyse e.V.
Albert-Einstein-Straße 29a, 18059 Rostock (Germany)
E-mail: matthias.beller@catalysis.de

[b] Dr. S. Dastgir, Dr. M. Anwar
Qatar Environment and Energy Research Institute (QEERI)
Hamad Bin Khalifa University (HBKU)
34110 Qatar Foundation, Doha (Qatar)

[c] Dr. R. Mocci
Dipartimento di Scienze Chimiche e Geologiche
Universitá degli Studi di Cagliari, SS 554 bivio per Sestu
09042 Monserrato (Italy)

[d] Dr. S. Bachmann, Dr. M. Scalone
Department of Process Chemistry and Catalysis
F. Hoffmann-La Roche Ltd., Grenzacherstrasse 124, 4070 Basel (Switzerland)

💻 Supporting information and the ORCID identification number(s) for the
author(s) of this article can be found under:
https://doi.org/10.1002/chem.202001866.

Part of a Special Issue celebrating the 1000th Issue of Chemistry—A European Journal.

**Chemistry–A European Journal**

Full Paper
doi.org/10.1002/chem.202001866

**Chemistry Europe**
European Chemical
Societies Publishing

cles,[4–6] a selection of potential catalytic materials was prepared.

As depicted in Figure 1A, after in situ generation of a Co(OAc)$_2$·4H$_2$O/chitin mixture, different metal oxides were added and stirred for 24 h. Afterwards, the solvent was removed and the obtained solids were pyrolysed at three different temperatures (600 °C, 700 °C and 800 °C with a temperature ramp of 25 °C min$^{-1}$) under Ar atmosphere for 2 h (for detailed preparation protocol the reader is referred to the Supporting Information).[9] The resulting materials possess a cobalt content of around 2 wt.% (Table S1). The activity of all these heterogeneous catalysts was evaluated in the benchmark hydrogenation of benzonitrile **1a** to benzylamine **2a**. In general, nitrile hydrogenation represents an important transformation in the bulk and fine chemical industry, since it furnishes primary amines that constitute key building blocks for the preparation of active pharmaceutical ingredients (APIs), life-science molecules, polymers, agrochemicals and dyes. Conventionally, such transformations under industrial conditions are conducted mostly applying skeletal catalysts such as Raney®-Ni and Raney®-Co or supported noble-metals such as Pd, Pt, Ru, Rh and Ir.[10] The increasing scarcity and price of the latter and the hazardous nature of the former create interest discovering less expensive and more sustainable catalysts. So far, the cobalt-catalyzed direct hydrogenation of nitriles has been scarcely explored and the corresponding catalysts were prepared using more expensive and special starting materials (see Scheme S2 for a summary of the previous works).[11–14]
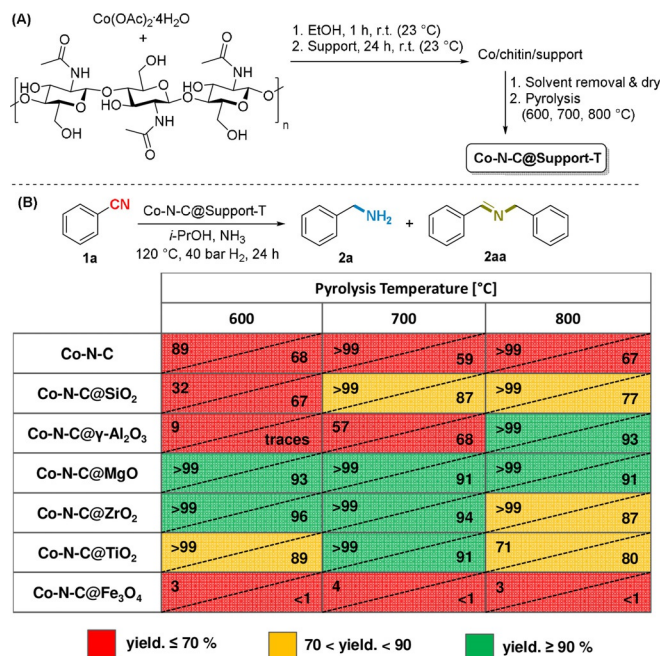
The results of the preliminary tests are summarized in Figure 1B. As shown by the color-code, it is immediately clear that both the pyrolysis temperature and the support are crucial for the reaction outcome. Without support, the resulting materials (Co-N-C) were not selective in the desired transformation, even if ammonia was added, which is known to suppress the undesired secondary imine **2aa** formation (see Scheme S1 for general reaction pathway).[10] Apart from Fe$_3$O$_4$-supported materials, which were completely inactive, addition of SiO$_2$, Al$_2$O$_3$, MgO or TiO$_2$ in general improved the selectivity. In order to distinguish more appropriately, the catalysts showing best performances (**2a** yield ≥ 90 %, green color-code) were studied under milder conditions (80 °C, 20 bar H$_2$). Here, all catalysts based on MgO outperformed the other materials and preserved good activity. In particular, Co-N-C@MgO-700 (treated at 700 °C) still showed complete conversion accompanied with a very high selectivity for benzyl amine **2a** even at 20 bar H$_2$ pressure (see Figure S20, Figure S21, and Figure S22). To investigate the reaction in more detail, different solvents have been employed and the proper ammonia concentration was determined (Figure S23 and Figure S24, respectively). In general, iPrOH in the presence of 1 M ammonia allowed for the best performance in terms of activity and selectivity. Clearly, no catalytic behavior was ruled out in the absence of catalysts or hydrogen (entries 2 and 3, Table S5). Notably, the formation of the composite material is crucial for product formation, as neither the unpyrolysed material nor the one prepared without the addition of chitin (entries 4 and 5, Table S5) showed activity. As expected, doped-carbon/MgO composites assembled without the addition of Co were inactive (entries 6–10, Table S5). All these experiments pointed out the importance of the synergistic combination of cobalt, carbon matrix and metal oxide. Systematic variation of the individual components of the carbon–magnesium oxide composite by changing the ratio between chitin and MgO from 1:3 to 3:1 followed by thermal treatment at 600, 700, and 800 °C (Figure S25) revealed optimal results of the catalyst prepared using a 1:1 mass ratio and pyrolysed at 700 °C (Co-N-C@MgO-700). Composition/time chart for this optimal catalyst (Figure S26) showed complete conversion (> 99 %) and excellent selectivity (98 %) at comparably low temperature (80 °C) over 24 h. With regard to selectivity, it is interesting to notice that N-benzylidenebenzylamine **2aa** is formed as intermediate during the reaction.[14, 15] Accordingly, if **2aa** was subjected to the standard reaction conditions, **2a** is formed with full conversion and almost complete selectivity (entry 1, Table S6).

Next, we compared the performance of Co-N-C@MgO-700 with state-of-the art systems, such as currently employed commercial heterogeneous catalysts, and related materials prepared from biopolymers (chitosan and cellulose). As depicted in Figure S27, the latter materials and previously reported cobalt nanoparticles on various supports showed inferior results. Similarly, our catalyst proved to be superior, even if compared with standard industrial catalysts including Raney-Ni as well as noble metal systems. Despite the good activities of noble-metal based catalysts in terms of conversion, selectivity in the desired primary amine was low or negligible due to the



**Figure 1.** Catalytic hydrogenation of benzonitrile (**1a**) to benzylamine (**2a**) and N-benzylidenebenzylamine (**2aa**). The numbers in each cell represent the conversion of **1a** (left) and the selectivity in **2a** (right). Color-code is based on **2a** yield. Reaction conditions: 0.5 mmol PhCN, 15 mg catalyst (1 mol% Co), 2 mL iPrOH, 200 μL aq. NH$_3$ (from a 25 % aqueous solution), 120 °C, 40 bar H$_2$, 24 h. Conversion and selectivities were determined using GC (n-hexadecane as internal standard).

formation of various side products. In particular, in the case of Pt/C, Raney-Ni and Ru/C the main side products were *N*-benzylidenebenzylamine **2 aa** and dibenzylamine **2 aaa**. When Pd/C and Pd(OH)$_x$/C were employed, along with **2 aa** and **2 aaa**, cyclohexylmethanamine and bis(cyclohexylmethyl)amine were detected by GC-MS indicating partial reduction of the arene ring.

Having an optimal material in hand, its reusability was examined. Gratifyingly, no loss of activity was detected in six additional runs (Figure S28). In agreement with this observation, cobalt leaching (both for active or inactive Co species) was ruled out after the sixth run by measuring the metal content in the liquid phase and performing Maitlis' hot filtration test (Table S7).

Because of their activity and selectivity in the desired transformation, especially materials based on MgO were characterized by means of X-ray powder diffraction (XRPD), X-ray photoelectron spectroscopy (XPS, ESCA), temperature programmed reduction (TPR-H$_2$) and transmission electron microscopy (TEM). Chemical composition analyses (CHN) of Co-N-C@MgO pyrolysed at different temperatures revealed constant values for all the elements except for nitrogen which showed a decreasing trend with the increase of the pyrolysis temperature (Table S1 and Table S2). Specific BET areas (SBET) were determined by N$_2$ adsorption/desorption isotherms (Figure 2 A and Figure S1). All the catalysts prepared with chitin displayed a type IV isotherm (according to IUPAC classification) typical for mesoporous materials. In contrast, Co@MgO-700 showed a type II isotherm indicating a nonporous material. As expected, the SBET depends on the pyrolysis temperature and a gradual decreasing is noticed with the increase of the pyrolysis temperature (Table S4 and Figure S3). In X-ray powder diffractograms the presence of MgO reflections (periclase) at $2\theta$ values around 37, 43, 63, 74, and 78° is dominant (Figure S4A).[16] In all the materials belonging to Co-N-C@MgO-T, MgO crystallite size (calculated via Scherrer equation) is around 41 nm, which is very close to the one calculate for the non-pyrolysed materials (42 nm). Apart from these signals, Co-N-C@MgO-800

showed a small diffraction peak at around $2\theta$ of 44° ascribed to Co$^0$.[17] An analogous situation is observed for Co-N-C(CE)@MgO-700, Co-N-C(CH)@MgO-700 and Co@MgO-700 (Figure S4B and S4C). In contrast, the material prepared without support (Co-N-C-700, Figure S4C) showed the exclusive presence of metallic Co ($2\theta$ values of around 44, 52 and 76°) and graphitic carbon ($2\theta$ value of 26°). Here, no crystalline cobalt oxides diffraction lines (Co$_3$O$_4$ or CoO) were observed by XRPD, which is in sharp contrast to previously known cobalt catalysts.[4,6] Exploring the near-surface composition of the materials by means of XPS, the Co2p core level spectrum of Co-N-C@MgO-T is characterized by two distinct components, Co2p$_{3/2}$ and Co2p$_{1/2}$ with peaks at around 781 eV and 798 eV, respectively (Figure 2 C). Each of them showed a shake-up satellite located about 7 eV above the primary emission peak and a spin-orbit separation ($\Delta E$ Co2p$_{1/2}$-Co2p$_{3/2}$) of 15.3 eV. This is in agreement with the presence of Co in +2 oxidation state.[17] Contrariwise, Co-N-C-700 and Co@MgO-700 exhibited different peaks (Figure S5C). In particular, Co-N-C-700 displayed a signal at 778.2 eV which is typical for cobalt in zero oxidation state, while Co@MgO-700 showed signals at higher binding energies (782.3 eV and 796.8 eV for Co2p3/2 and Co2p$_{1/2}$, respectively) indicating oxidized Co species.[18] The material prepared with chitosan (Co-N-C(CH)@MgO-700) exhibited a similar pattern to Co-N-C@MgO-700, whereas Co-N-C(CE)@MgO-700 prepared from cellulose displayed peaks slightly shifted towards lower binding energies indicating a possible reduction of Co$^{II}$ (Figure S5B). Deconvolution of the N1s region for Co-N-C@MgO-T revealed the presence of two signals at 398 eV (pyridinic nitrogen or Co-N$_x$ functionalities) and 400.8–401.2 eV (pyrrolic or graphitic N configurations) for each catalyst (Figure S6 and Figure 2 D).[19] Notably, a decreasing of the intensity of the peak centered at 398 eV and an increasing and broadening of the one centered at 401 eV can be detected with the increasing of the pyrolysis temperature, which is in agreement with the structural evolution of pyridinic to graphitic N functionalities in doped carbonaceous materials upon heating.[20] Similar distribution of the N1s peaks have been detected in Co-N-C-700 and N-C@MgO-700 (Figure S6B). Analysis of the Mg1s core revealed the presence of three deconvolution peaks (around 1303, 1304.5 and 1305.5 eV, respectively) for each material that can be ascribed to the presence of Mg$^{II}$ in the bulk (Mg$^{2+}$ O$^{2-}$), on the surface (-O-Mg(OH)-O-), and as MgCO$_3$ (Figure S7).[21] The presence of the latter two species is not surprising since magnesium oxide possess surface chemisorbed OH groups, which are retained also at high temperature (up to 1200 °C).[22] In addition, pyrolysis of chitin partially produces CO$_2$ and water giving rise to the partial formation of MgCO$_3$ and Mg(OH)$_2$. Carbon C1s core showed, along with the reference carbon peak at 284.8 eV (ascribed to C—C bonds), the presence of other C—X or C=X (X = N, O) functionalities, which signals are located at higher binding energies (Figure S8). The C1s XPS patterns are very similar for all the characterized catalysts, except for the unpyrolysed material (Co(OAc)$_2$-Chitin-MgO) that showed numerous peaks, which reflect the presence of chitin carbon atoms in different electronic environments. Finally, regarding the O1s region, deconvolution generated three
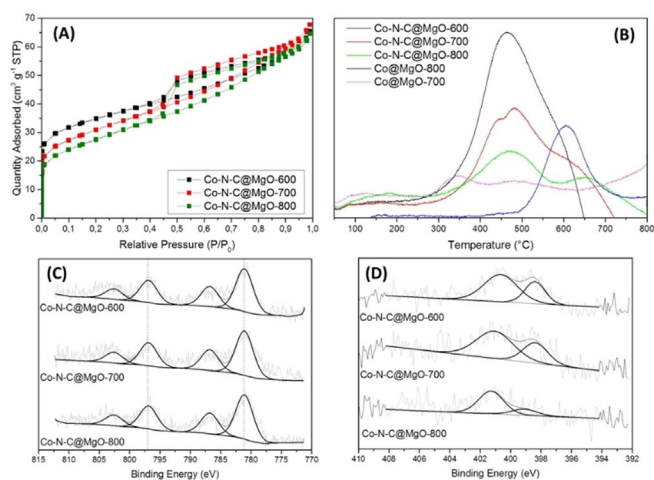


**Figure 2.** N$_2$ adsorption–desorption isotherms (A), TPR-H$_2$ patterns (B), Co2p XPS (C) and N1s XPS (D) of selected catalytic materials.

peaks for all the analyzed materials (Figure S9); however, a rigorous assignment was not possible. It should be anyway noted that the treatment of MgO with water or $CO_2$-enriched atmospheric air led to the formation of three O1s peaks after deconvolution (530 eV, 532 eV, and 533 eV), which were ascribed to bulk magnesium oxide, superficial magnesium hydrates, and magnesium carbonates, respectively.[23] The reducibility of the catalysts has been elucidated using temperature-programmed reduction technique (TPR-$H_2$). As depicted in Figure 2B, Co-N-C@MgO-T catalysts showed a main signal at around 475 °C, which is typical for the reduction of cobalt oxides in N-doped graphene matrix.[24] On the contrary, Co@MgO-700 showed two peaks at around 350 °C and 475 °C indicating the presence of two reducible Co species. According to the literature, these can be assigned to the two-steps reduction of supported $Co_3O_4$ ($Co_3O_4 \rightarrow CoO \rightarrow Co$), which is in accordance with XPS (vide supra).[25] Surprisingly, Co@MgO-800 showed a totally different pattern: A unique peak centered at 600 °C was detected indicating the presence of difficulty reducible Co species. These can be attributed to Mg/Co spinels ($MgCo_2O_4$) or MgO/$CoxOy$ solid solutions.[26] Interestingly, it should be noted that Co-N-C@MgO-700 showed a shoulder in the 600–650 °C region that became a defined peak in Co-N-C@MgO-800 indicating the partial formation of spinels and/or mixed oxides in the Co-N-C@MgO-T materials, too. The decreasing of reducibility of the latter samples has been also confirmed by the reduced amount of consumed $H_2$ in the TPR experiments (Figure S10).

To further elucidate structural, electronic, and morphological properties of various prepared materials, transmission electron microscopy was performed. TEM investigations of the cobalt-free N-C@MgO-700 sample showed the formation of variously sized MgO nanocubes (size of around 100 nm) bringing carbonaceous structures regularly distributed on them (Figure S11). Similarly, catalyst Co-N-C@MgO-600 showed both the presence of MgO nanocubes and extended carbonaceous structures (see Figure S12). Various Co NPs (10–20 nm size) were found to be well distributed on the latter structures and a negligible amount of them were present on or in the proximity of the MgO (Figure 3 and Figure S12). Additionally, some agglomerated Co phases were present on the edges of the carbon phase (Figure S12K). Moving to Co-N-C@MgO-700 and Co-N-C@MgO-800, Co NPs were located both on the carbon matrix and on the MgO cubes (Figure S3D–F and G–I), which in this case have a size up to 100 nm. Interestingly, TEM mapping clearly shows that the Co NPs on the latter phase are smaller than the one present on the former, reaching down to 10 nm (compare Figure S13H with Figure S13K, and Figure S14H with Figure S14K). This can be ascribed to the ability of MgO to homogeneously disperse metal species.[27] Moreover, moving from pyrolysis temperature from 700 °C to 800 °C a general increasing of the particle size is observed (agglomeration). It is important to further notice that all the Co NPs are embedded within various layers of ordered graphenic-like carbon structures. The catalyst Co-N-C-700 also showed the presence of Co NPs on carbon (Figure S15). However, the dispersion is not homogeneous as in the case of Co NPs located on MgO and a variety of Co particles ranging between 10–100 nm NPs are clearly visible (Fig-
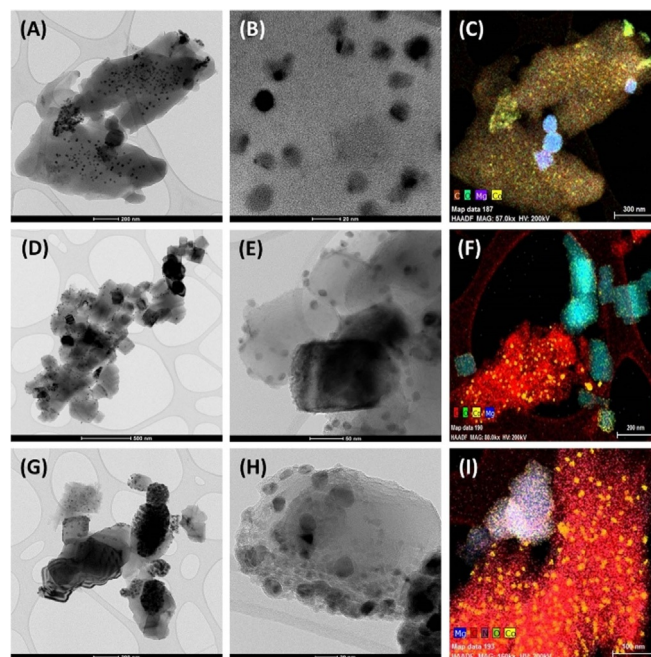


**Figure 3.** TEM images of Co-N-C@MgO-600 (A, B, C), Co-N-C@MgO-700 (D, E, F) and Co-N-C@MgO-800 (G, H, I).

ures S15B and S15I). The material prepared without chitin, Co@MgO-700 (not active in the desired transformation) displayed a totally different composition (Figure S16). Variously shaped (cubes, rectangles, finger-like) MgO structures were present and no visible Co NPs could be detected. However, TEM mapping shows a uniform dispersion of Co species on the magnesium oxide support (compare Figure S16F and S16G). This corroborates the postulated formation of a Mg/Co spinels ($MgCo_2O_4$) or MgO/$CoO_x$ solid solutions on the base of the XRPD, TPR-$H_2$ and XPS results (vide supra).

Finally, the catalysts prepared using cellulose (Co-N-C(CE)@MgO-700) and chitosan (Co-N-C(CH)@MgO-700) as carbon precursors were analyzed (Figure S17 and Figure S18). In both cases, mapping showed that variously sized Co NPs are preferentially located on the carbon phase leaving the MgO phase almost unloaded. In addition, agglomeration of the particles is detected. Both the latter features could be the reason for the decreased activity of Co-N-C(CE)@MgO-700 and Co-N-C(CH)@MgO-700. On the base of the previous we could assume that the proposed spinels or solid solution play a minor or negligible role in the catalytic event. On the other hand, particle size and their location play a significant role. As a result, catalyst Co-N-C@MgO-700, which shows the best catalytic activity, shows both small Co NPs which are preferentially located on MgO. Lastly, the catalyst recovered after five recycling runs has been also characterized. TEM analysis still showed the presence of Co diffused Co species both on carbon matrix and MgO phase. Additionally, as shown in Figure S19, XPS analysis revealed a very similar peak distribution if compared with the fresh material with small differences detected only for the O1s region (Figure S19).

With a suitable catalyst and conditions in hand, scope and limitations of the described protocol were explored starting with substituted aryl nitriles (Figure 4). Substrates bearing electron-donating (**1b**, **1c**, **1e**) or electron-withdrawing (**1d**) groups in *para-* position were smoothly converted to the corresponding benzyl amines at 80 °C or 100 °C in very high yields. Except for 4-iodobenzonitrile (**1j**), all other halide-containing nitriles (**1g**, **1h**, **1i**) did not pose any selectivity problems and furnished the desired products in >98% yield. In case of *ortho*-substitution good product yields (**2k**, **2l**, **2m**, **2n**) were achieved at slightly higher reaction temperature and/or catalyst loading. Dinitriles are common starting materials for the preparation of important building blocks for polymer production. Hence, 1,3- and 1,4-phenylenedimethanamines (**2o** and **2p**) were produced following our protocol. Interestingly, more functionalized substrates containing carboxylic acid derivatives such as esters (**1q**), phthalides (**1r**) or amides (**1s**, **1u**) including biologically relevant β-lactam scaffold (**1x**) were converted into the corresponding aryl amines maintaining the integrity of the residual moieties. Furthermore, amino groups are tolerated to give the corresponding diamino compounds (**2m**, **2c**). In addition, piperonylonitrile (**1y**) and 4-benzyloxybenzonitrile (**1z**) yielded the corresponding products
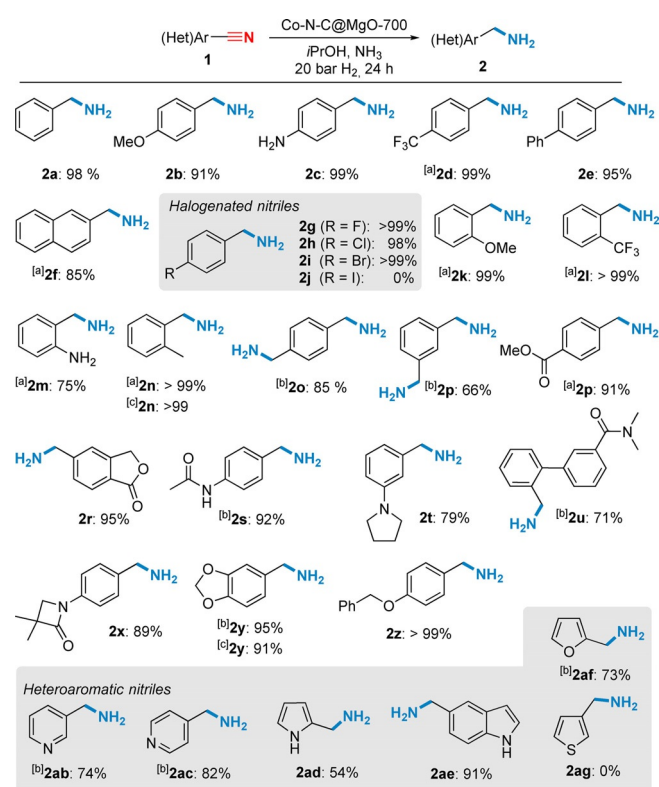
in almost quantitative yield. Surprisingly, no cleavage of the C—O bond was observed, despite the lability of the benzyl ether moiety in the presence of hydrogen and metal catalysts. Except for thiophene,[11] a selection of heteroaromatic nitriles based on pyridine (**1ab**, **1ac**), pyrrole (**1ad**), indole (**1ae**), and furan (**1af**) were hydrogenated to the corresponding primary amines in good yields, too. The sluggish reactivity showed by **1ag** was imputed by the poisoning effect of the sulfur atom. In fact, the hydrogenation of benzonitrile **1a** conducted in the presence of thiophene is completely inhibited (Table S8). While most of the catalytic experiments (vide supra) have been performed under mild conditions, it is possible to lower the reaction temperature further on, which might be useful for pharmaceutical applications. In fact, mild operative temperatures are not only relevant in terms of energy saving but also due to safety aspects in the scale-up process. As exemplified by reactions of **1n** and **1y**, very good product yields were obtained even below 80 °C. Limitations to the reported protocol were detected in the case of nitriles containing C=C double bonds, nitro group and ketones. In these cases, the nitrile group is reduced along with the second functionality giving rise to a mixture of products (Scheme S3).

To demonstrate the advantages of this novel catalyst system the hydrogenation of picolinonitrile (**1ah**) (2-pyridinecarbonitrile) was investigated. Noteworthy, the selective reduction of this particular substrate fails even with noble-metal catalysts such as Pd.[28] The specific problem in this hydrogenation is explained by preferential hydrolysis to picolinamide (**2aah**) due to an anchimeric assistance of the heterocyclic nitrogen atom adjacent to the nitrile group.[29] While poor conversion and selectivity were obtained at 80 °C (Table 1, entry 1), reaction at higher temperature and increased catalyst loading in the presence of Et₃N as base afforded the desired primary amine with a selectivity of 70% (Table 1, entry 2). With other metal catalysts based on Pd, Pt or Ru much lower selectivity and mainly over-hydrogenated products were obtained (Table 1, entries 3–6).



**Figure 4.** Hydrogenation of aryl and heteroaryl nitriles: Reaction scope. Reaction conditions: 0.5 mmol PhCN, 15 mg catalyst (1 mol% Co), 2 mL *i*PrOH, 200 µL aq. NH₃ (from a 25% aqueous solution), 80 °C, 20 bar H₂, 24 h. [a] Reaction was conducted at 100 °C. [b] Reaction was conducted at 110 °C using 30 mg of catalysts (2 mol% Co). [c] Reaction was conducted at 70 °C using 45 mg of catalyst (3 mol% Co). Products **2f**, **2p**, **2r**, **2x** and **2o** were obtained as hydrochloric salts. Products **2s**, **2z**, **2u** were isolated as primary amines. Remaining product yields were determined using GC (*n*-hexadecane as internal standard).

**Table 1.** Hydrogenation of picolinonitrile **1ah**.[a]



| Entry | Catalyst amount [mg] (Co mol%) | Temp. [°C] | H₂ [bar] | 1ah Conv. [%] | 2ah Sel. [%] | 2aah Sel. [%] |
|---|---|---|---|---|---|---|
| 1 | 15 (1) | 80 | 20 | 26 | 22 | 70 |
| 2[b] | 45 (3) | 130 | 40 | >99 | 70 | 25 |
| 3[b] | 10% Pd/C | 130 | 40 | >99 | <1 | <1 |
| 4[b] | 10% Pd(OH)ₓ/C | 130 | 40 | >99 | <1 | <1 |
| 5[b] | 10% Pt/C | 130 | 40 | >99 | 31 | <1 |
| 6[b] | 5% Ru/C | 130 | 40 | >99 | 49 | <1 |

Reaction conditions: [a] 0.5 mmol picolinonitrile **1ah**, 2 mL *i*PrOH, 200 µL aq. NH3 (from a 25% aqueous solution), 24 h. Conversion and selectivities were determined using GC (*n*-hexadecane as internal standard). [b] 373 µL Et₃N and 140 µL H₂O were used instead of NH₃. Complete mass balance is given by the formation of (*E*)-1-(pyridin-2-yl)-*N*-(pyridin-2-ylmethyl)methanimine that has been detected by GC-MS.
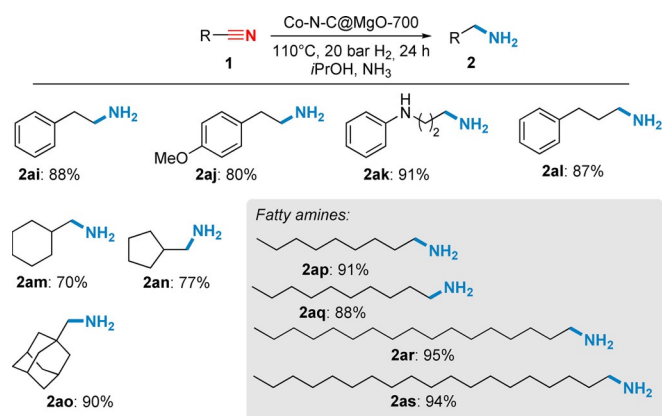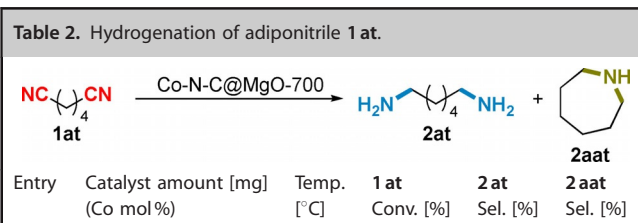
**Figure 5.** Hydrogenation of aliphatic nitriles: Reaction scope. Reaction conditions: 0.5 mmol substrate, 30 mg catalyst (2 mol% Co), 2 mL *i*PrOH, 200 μL aq. NH₃ (from a 25% aqueous solution), 110 °C, 20 bar H₂, 24 h. Product **2 ak** was obtained as hydrochloric salt. Products **2 ao**, **2 aq**, **2 ar** and **2 as** were isolated as primary amines. Remaining product yields were determined using GC (*n*-hexadecane as internal standard).



**Table 2.** Hydrogenation of adiponitrile **1 at**.

| Entry | Catalyst amount [mg] (Co mol%) | Temp. [°C] | 1 at Conv. [%] | 2 at Sel. [%] | 2 aat Sel. [%] |
|---|---|---|---|---|---|
| 1 | 15 (1) | 80 | 47 | < 1 | 95 |
| 2 | 45 (3) | 80 | > 99 | 95 | < 1 |
| 3 | 30 (2) | 110 | > 99 | 98 | < 1 |

Reaction conditions: 0.5 mmol adiponitrile **1 at**, 2 mL *i*PrOH, 200 μL aq. NH₃ (from a 25% aqueous solution), 20 bar H₂, 24 h. Conversion and selectivities were determined using GC (*n*-hexadecane as internal standard).

Next, we investigated the reactivity of aliphatic nitriles (Figure 5), which require harsher conditions. Nevertheless, benzyl cyanides (**1 ai** and **1 aj**), other aliphatic (**1 ak**, **1 al**) and alicyclic (**1 am**, **1 an**, **1 ao**) nitriles were smoothly hydrogenated affording the corresponding amines in good yields. Furthermore, we applied our protocol for the synthesis of industrially relevant aliphatic amines such as fatty amines and 1,6-diaminohexane. Longer chain alkyl amines are applied in adhesive formulations, softeners, emulsifiers and flotation agents (corresponding salts).[30] These so-called fatty amines are usually produced on large scale by the so-called Nitrile Process in the presence of Raney-Ni, Raney-Co or copper-chromite catalysts.[31] Gratefully, Co-N-C@MgO-700 successfully catalyzed this transformations at 110 °C and 20 bar hydrogen giving the products in excellent yield. It should be mentioned here that the products were obtained straightforward in a pure form after simple filtration over Celite for catalyst removal and consecutive solvent evaporation.

The reaction of adiponitrile (**1 at**) to hexamethylenediamine, which is used as monomer for the production of Nylon 6.6 and other related polymers, represents the largest nitrile hydrogenation in industry. The current process uses Raney-Ni (low pressure process) or promoted cobalt, iron oxides (high pressure process) as catalysts and the desired product is obtained with a selectivity of about 90%.[32] Interestingly, under our standard conditions azepane (**2 aat**) is formed in high selectivity (95%). However, by increasing either the temperature and/or the catalyst loading (Table 2, entries 2 and 3) the desired product is obtained in high conversion and selectivity (> 99% and 98%, respectively).

Finally, the utility of our developed protocol was also tested in some gram-scale reactions (scaled-up by a factor of 25). As depicted in Scheme S4, the obtained yields were comparable to the ones obtained in 0.5 mmol scale.

## Conclusions

Cobalt nanoparticles were supported on several carbon/metal oxide hybrid materials, which are easily generated from inexpensive and easily available chitin and the corresponding metal oxides. This concept allows the preparation of unique materials, which are of interest for all kinds of green catalytic transformations. The presented methodology displays broad scope and functional group tolerance, including the selective hydrogenation of industrially significant aromatic and aliphatic nitriles.

Among this novel class of composites, specifically Co-N-C@MgO-700 was able to catalyze the hydrogenation of diverse nitriles to primary amines in high yields and often under very mild conditions (> 40 examples). Comparison of Co-N-C@MgO-700 to noble metal-based catalysts for selected examples demonstrates the improved performance of this novel material. Characterization reveals the importance of Co NPs both on the carbon matrix and on the MgO cubes.

**Chemistry–A European Journal**

Full Paper
doi.org/10.1002/chem.202001866

**Chemistry Europe**
European Chemical
Societies Publishing

## Conflict of interest

The authors declare no conflict of interest.

[1] X. Cui, W. Li, P. Ryabchuk, K. Junge, M. Beller, *Nat. Catal.* **2018**, *1*, 385–397.

[2] M.-M. Titirici, M. Antonietti, *Chem. Soc. Rev.* **2010**, *39*, 103–116.

[3] N. Yan, X. Chen, *Nature* **2015**, *524*, 155–157.

[4] B. Sahoo, D. Formenti, C. Topf, S. Bachmann, M. Scalone, K. Junge, M. Beller, *ChemSusChem* **2017**, *10*, 3035–3039.

[5] F. K. Scharnagl, M. F. Hertrich, F. Ferretti, C. Kreyenschulte, H. Lund, R. Jackstell, M. Beller, *Sci. Adv.* **2018**, *4*, eaau1248.

[6] B. Sahoo, A.-E. Surkus, M.-M. Pohl, J. Radnik, M. Schneider, S. Bachmann, M. Scalone, K. Junge, M. Beller, *Angew. Chem. Int. Ed.* **2017**, *56*, 11242–11247; *Angew. Chem.* **2017**, *129*, 11394–11399.

[7] A. Borenstein, O. Hanna, R. Attias, S. Luski, T. Brousse, D. Aurbach, *J. Mater. Chem. A* **2017**, *5*, 12653–12672.

[8] W.-D. Lu, Q.-N. Wang, L. He, W.-C. Li, F. Schüth, A.-H. Lu, *ChemNanoMat* **2018**, *4*, 505–509.

[9] R. V. Jagadeesh, T. Stemmler, A.-E. Surkus, M. Bauer, M.-M. Pohl, J. Radnik, K. Junge, H. Junge, A. Bruckner, M. Beller, *Nat. Prot.* **2015**, *10*, 916–926.

[10] D. B. Bagal, B. M. Bhanage, *Adv. Synth. Catal.* **2015**, *357*, 883–900.

[11] F. Chen, C. Topf, J. Radnik, C. Kreyenschulte, H. Lund, M. Schneider, A.-E. Surkus, L. He, K. Junge, M. Beller, *J. Am. Chem. Soc.* **2016**, *138*, 8781–8788.

[12] P. Ji, K. Manna, Z. Lin, X. Feng, A. Urban, Y. Song, W. Lin, *J. Am. Chem. Soc.* **2017**, *139*, 7004–7011.

[13] R. Ferraccioli, D. Borovika, A.-E. Surkus, C. Kreyenschulte, C. Topf, M. Beller, *Catal. Sci. Technol.* **2018**, *8*, 499–507.

[14] K. Murugesan, T. Senthamarai, M. Sohail, A. S. Alshammari, M.-M. Pohl, M. Beller, R. V. Jagadeesh, *Chem. Sci.* **2018**, *9*, 8553–8560.

[15] P. Ryabchuk, G. Agostini, M.-M. Pohl, H. Lund, A. Agapova, H. Junge, K. Junge, M. Beller, *Sci. Adv.* **2018**, *4*, eaat0761.

[16] M. A. Aramendía, J. A. Benítez, V. Borau, C. Jiménez, J. M. A. Marinas, J. R. Ruiz, F. Urbano, *J. Solid State Chem.* **1999**, *144*, 25–29.

[17] D. Formenti, F. Ferretti, C. Topf, A.-E. Surkus, M.-M. Pohl, J. Radnik, M. Schneider, K. Junge, M. Beller, F. Ragaini, *J. Catal.* **2017**, *351*, 79–89.

[18] T. D. M. Elko-Hansen, J. G. Ekerdt, *Chem. Mater.* **2014**, *26*, 2642–2646.

[19] F. Jaouen, J. Herranz, M. Lefèvre, J.-P. Dodelet, U. I. Kramm, I. Herrmann, P. Bogdanoff, J. Maruyama, T. Nagaoka, A. Garsuch, J. R. Dahn, T. Olson, S. Pylypenko, P. Atanassov, E. A. Ustinov, *ACS Appl. Mater. Interfaces* **2009**, *1*, 1623–1639.

[20] J. R. Pels, F. Kapteijn, J. A. Moulijn, Q. Zhu, K. M. Thomas, *Carbon* **1995**, *33*, 1641–1653.

[21] M. M. Natile, A. Glisenti, *Surf. Sci. Spectra* **2006**, *13*, 17.

[22] S. Ardizzone, C. L. Bianchi, M. Fadoni, B. Vercelli, *Appl. Surf. Sci.* **1997**, *119*, 253–259.

[23] V. Rheinheimer, C. Unluer, J. Liu, S. Ruan, J. Pan, P. J. M. Monteiro, *Materials* **2017**, *10*, 75–91.

[24] Z. Wei, J. Wang, S. Mao, D. Su, H. Jin, Y. Wang, F. Xu, H. Li, Y. Wang, *ACS Catal.* **2015**, *5*, 4783–4789.

[25] S. Karimi, A. Tavasoli, Y. Mortazavi, A. Karimi, *Appl. Catal. A* **2015**, *499*, 188–196.

[26] H. Y. Wang, E. Ruckenstein, *Carbon* **2002**, *40*, 1911–1917.

[27] W. Liu, L. Zhang, W. Yan, X. Liu, X. Yang, S. Miao, W. Wang, A. Wang, T. Zhang, *Chem. Sci.* **2016**, *7*, 5758–5764.

[28] M. Vilches-Herrera, S. Werkmeister, K. Junge, A. Börner, M. Beller, *Catal. Sci. Technol.* **2014**, *4*, 629–632.

[29] M. Honda, M. Tamura, K. Nakao, K. Suzuk, Y. Nakagawa, K. Tomishige, *ACS Catal.* **2014**, *4*, 1893–1896.

[30] P. Foley, A. Kermanshahipour, E. S. Beach, J. B. Zimmerman, *Chem. Soc. Rev.* **2012**, *41*, 1499–1518.

[31] J. Barrault, Y. Pouilloux, *Catal. Today* **1997**, *37*, 137–153.

[32] B. D. Herzog, R. A. Smiley, in *Ullmann's Encyclopedia of Industrial Chemistry*, Wiley-VCH, Weinheim, **2012**.